Effects of rising amyloidβ levels on hippocampal synaptic transmission, microglial response and cognition in *APP*$_{Swe}$/*PSEN1*$_{M146V}$ transgenic mice

Ms Evelyn Medawar MSc* (medawar@cbs.mpg.de)
Dr Tiffanie Benway PhD* (tiffanie.benway@smallpharma.co.uk)
Dr Wenfei Liu PhD* (wenfei.liu.10@ucl.ac.uk)
Mr Taylor A. Hanan MSc (taylor.a.hanan@gmail.com)
Dr Peter Haslehurst PhD (peter.haslehurst@pharm.ox.ac.uk)
Dr Owain T. James PhD (owain.t.james@gmail.com)
Mr Kenrick Yap, MSc (kenrkyap@gmail.com)
Dr Laurenz Muessig PhD (l.mussig@ucl.ac.uk)
Ms Fabia Moroni MSc (fabia.moroni@gmail.com)
Dr Muzzamil A. Nahaboo Solim, MSBS (muzammil.solim.09@ucl.ac.uk)
Ms Gaukhar Baidildinova MSc (baidildag@mail.ru)
Ms Rui Wang (r.wang@ucl.ac.uk)
Dr Jill C. Richardson PhD§ (jillyrichardson@ntlworld.com)
Dr Francesca Cacucci PhD (f.cacucci@ucl.ac.uk)
Dr Dervis A. Salih PhD (dervis.salih@ucl.ac.uk)
Dr Damian M. Cummings PhD† (d.cummings@ucl.ac.uk)
Prof Frances A. Edwards PhD† (f.a.edwards@ucl.ac.uk)

***Joint first authors**
†Joint corresponding authors

University College London, Gower Street, London, WC1E 6BT, UK
§ Neurosciences Therapeutic Area, GlaxoSmithKline R&D, Gunnels Wood Road, Stevenage, SG1 2NY, UK

Abstract

Background

Progression of Alzheimer's disease is thought initially to depend on rising amyloidβ and its synaptic interactions. Transgenic mice (TASTPM; $APP_{\mathrm{Swe}}/PSEN1_{\mathrm{M146V}}$) show altered synaptic transmission, compatible with increased physiological function of amyloidβ, before plaques are detected. Recently, the importance of microglia has become apparent in the human disease. Similarly, TASTPM show a close association of plaque load with upregulated microglial genes.

Methods

CA1 Synaptic transmission and plasticity were investigated using *in vitro* electrophysiology. Migroglial relationship to plaques was examined with immunohistochemistry. Behaviour was assessed with a forced-alternation T-maze, open field, light/dark box and elevated plus maze.

Findings

The most striking finding is the increase in microglial numbers in TASTPM, which, like synaptic changes, begins before plaques are detected. Further increases and a reactive phenotype occur later, concurrent with development of larger plaques. Long-term potentiation is initially enhanced at pre-plaque stages but decrements with the initial appearance of plaques. Finally, despite altered plasticity, TASTPM have little cognitive deficit, even with a heavy plaque load, although they show altered non-cognitive behaviours.

Interpretation

The pre-plaque synaptic changes and microglial proliferation are presumably related to low, non-toxic amyloidβ levels in the general neuropil and not directly associated with plaques. However, as plaques grow, microglia proliferate further, clustering around plaques and becoming phagocytic. Like in humans, even when plaque load is heavy, without development of neurofibrillary tangles and neurodegeneration, these alterations do not result in cognitive deficits. Behaviours are seen that could be consistent with pre-diagnosis changes in the human condition.

Funding

GlaxoSmithKline; BBSRC; UCL; ARUK; MRC.

Keywords

Alzheimer's disease; dementia; mouse model; synaptic transmission; microglia; plaque; neurodegeneration.

Research in context

Evidence before this study

There is a large body of research examining many aspects of phenotypes associated with mouse models of Alzheimer's disease – a PubMed search for the terms Alzheimer* AND mouse returns in excess of 21000 articles. However, there are few systematic articles pulling together pathological, functional (electrophysiological), and behavioural analyses across the life-span of such models. There is also a number of conflicting outcomes, for example reports of impaired versus enhanced synaptic plasticity; cognitive impairments or not.

Recently, the importance of microglia in Alzheimer's disease has come to the fore in human Genome Wide Association Studies (GWAS), with variants of a number of microglial genes identified as risk-factors for developing the disease. Interestingly, we have recently reported that *Trem2* and other genes identified as risk-factors in humans are strongly up regulated in close association to plaque development in the mouse model used in this study. Moreover, this previous study predicted two of the most recently identified genes that were identified in GWAS since the publication of our paper.

We have previously used this model to identify the earliest synaptic changes and shown changes in release of glutamate, the primary excitatory neurotransmitter in the brain, to occur even before plaques are detectable.

Added value of this study

By studying this transgenic mouse model of Alzheimer's disease, throughout the development of plaques, from prior to detection through to heavy plaque loads, we have

been able to identify a clear time course of key phenotypic changes associated with early disease. In particular, this study identifies the very early changes in microglia and can separate the time course of the microglial phenotype. In addition, we detail the changes in synaptic plasticity over time and importantly identify that, like in humans in the absence of Tau tangles or neurodegeneration, considerable synaptic changes can occur and a heavy plaque load without resulting in substantial cognitive loss.

Implications of all the available evidence

Our data indicate that rising amyloid beta prior to detectable plaque deposition results in changes in synaptic function that likely reflects an enhanced physiological effect of amyloid beta. At this stage, microglia proliferate but do not activate. Once plaques begin to appear, microglia migrate to surround the plaque and become phagocytic, likely targeting dystrophic synapses and neurites caused by the cloud of highly-toxic amyloid beta around the plaque. Similarly to humans, who have plaques but no tangles and have yet to develop substantial neurodegeneration, cognitive deficits are not seen, even with a heavy plaque load; behavioural changes are limited to anxiety-like effects.

This investigation of the parallel time-course of events highlights the probability that, if progression of disease can be reversed or slowed early enough, before Tau tangles and substantial neurodegeneration occur, the symptoms of cognitive decline could be very largely avoided. Moreover, it suggests that the substantial increases in microglia number and upregulation of their specific gene expression in association with plaques, is not associated with cognitive loss and may indeed be protective.

Introduction

The onset and progression of Alzheimer's disease (AD) is most likely initiated by environmental factors interacting with predisposed genetic risks, many of which have now been identified in genome-wide association studies (see reference 1 for review). In familial AD, an inherited mutation causes rising amyloidβ (Aβ) levels and it has long been established that this triggers a chain of events that leads to the eventual cognitive decline.[2] In sporadic AD, it is highly likely that initial triggering events (genetic and/or environmental) also lead to rising Aβ and that, like in the familial disease, Aβ levels represent an essential contributor to the ongoing pathology and eventual neurodegeneration.[3, 4] Under normal physiological conditions, Aβ acts as an activity-dependent synaptic modulator which, when released from presynaptic neuronal terminals, increases probability of glutamate release.[5] Inappropriate neuronal activity and/or genetic imbalances in production versus clearance mechanisms may thus lead to a prolonged rise in Aβ levels,[6] enabling the formation of Aβ oligomers and deposition of plaques. It is notable that restoring γ-frequency oscillations in transgenic mouse models expressing genes harbouring familial mutations associated with familial AD, reduces Aβ load[7] and restores cognitive deficits.[8]

Animal models for AD have generally depended on transgenic expression, or more recently knock-in of the gene variants that cause the familial dominantly inherited forms of the disease, particularly amyloid precursor protein (*APP*) or presenilin 1 or 2 (*PSEN1* or *PSEN2*). This is an effective approach for initiating the rise in Aβ and the deposition of plaques, albeit by a different trigger than in sporadic AD. According to the 'amyloid hypothesis', in the human disease, rise in Aβ and plaque deposition is suggested to lead to altered neuronal ionic homeostasis and increased oxidative stress. Together, these may result in increased kinase activity on microtubule-associated protein Tau, resulting in Tau hyperphosphorylation and neurofibrillary tangle formation.[9] The exact mechanisms linking Aβ and Tau phosphorylation remain unclear and unfortunately, despite the initiation of Aβ pathology, mouse models with genes for familial Alzheimer's disease do not completely recapitulate these later events. As documented in the initial descriptions of the TASTPM mice, which are hemizygous for both human APP_{Swe} and human $PSEN1_{M146V}$, plaques are first detected at approximately 4 months of age and a considerable plaque load develops by 8 months.[10, 11] Furthermore, phosphorylation of

151 Tau is detectable in the dystrophic neurites around plaques,[11] recently suggested to be
152 an early stage of Tau pathology.[12] An inability to extinguish hippocampal-dependent
153 contextual fear conditioning at 4 months when plaques are first detected[13, 14] and a
154 deficit in novel object recognition at 6 months,[15] have also been reported.
155
156 We recently reported alterations in synaptic transmission preceding the detection of
157 plaques, manifesting as a loss of spontaneous action potentials in Schaffer collateral
158 axons and a concomitant increase in probability of glutamate release.[16] Importantly, we
159 have demonstrated an almost 1:1 correlation of plaque load with expression of a module
160 of microglial genes throughout the life of these and other transgenic mice. This
161 correlation in Aβ mice contrasts with the interaction of microglia and neurofibrillary
162 tangles in mice with Tau mutations, in which microglial genes are only upregulated with
163 advanced tangle load (www.mouseac.org).[10]
164
165 Here we extend our previous studies on TASTPM mice to understand the relationship
166 between early changes in synaptic transmission, synaptic plasticity, cognitive function
167 and microglia. We study the development of plaques in more detail and dissect out the
168 microglial response to distinguish between the numbers of microglia and their
169 phagocytic status. We find that, like synaptic changes, microglia are more prevalent even
170 before plaques are detectable, whereas their phagocytic phenotype is age-related,
171 coming much later. We then proceed to study hippocampal synaptic plasticity and
172 hippocampus-dependent learning, in the forced-alternation T-maze, enabling
173 identification of Aβ phenotypes, finding little cognitive deficit even with a heavy plaque
174 load but clear behavioural changes, probably related to increased levels of anxiety.
175 While we continue to focus mainly on the previously defined TASTPM mice (double
176 hemizygote), we have broadened the study to investigate dose dependency of the
177 transgene by including mice homozygous for both genes. The effect of the individual
178 genes is also investigated in mice with hemizygous expression of only one or the other
179 gene. When not otherwise defined, TASTPM mice hence refers to the double hemizygous
180 mouse.

Methods

Animals

All experiments were performed in agreement with the UK Animals (Scientific Procedures) Act 1986, with local ethical approval and in agreement with the GlaxoSmithKline statement on use of animals. Male TASTPM mice and C57Bl/6j mice were supplied by GlaxoSmithKline and bred either at Charles River Laboratories International, Inc. (Margate, UK) or at UCL by crossing male homozygous TASTPM with female C57Bl/6j. Age-matched, non-littermate male C57Bl/6j mice were used as wild type controls. In some experiments, double homozygous TASTPM were bred. Single mutant TAS (APP_{Swe})[17] or TPM ($PSEN1_{M146V}$)[15] mice were bred by crossing hemizygous parents. Mice from Charles River were shipped to UCL upon weaning at 21-days-old.

In this study we avoided single housing by keeping mice in large open cages (20 x 35 x 45 cm) and enriching their environments. Under these conditions, while the aggressive nature of the TASTPM mouse is not completely avoided, it is less of a problem and allows group housing to be maintained over the lifetime of the mice. Thus, cages containing 2-8 male mice were maintained in a 12-hour light/12-hour dark cycle with food (Envigo 2018 Teklad global 18% protein rodent diet) and water *ad libitum*. Environmental enrichment consisted of changes of food location, bedding type (e.g. tissue, shredded paper, paper roll, paper bags) and inanimate objects (e.g. running wheels, rodent balls, tubing, houses (mostly purchased from Eli Lilly Holdings Limited, Basingstoke, UK)) within the cage at least once per week. Mice were used for experimentation at the ages stated (± 0·5 months) and, where unavoidable, were single-housed for no longer than 24 hours. Tails or ear punches were used for genotyping by standard PCR protocols to ensure the presence of the expected genes.

Genotyping

Genotype confirmation using conventional PCR methods

Briefly, genomic DNA was extracted using the 'HotSHOT' lysis method. Alkaline lysis reagent (25 mM NaOH, 0·2 mM EDTA, pH12) was added to tissue samples prior to heating to 95°C for 30 minutes. The sample was then cooled to 4°C before the addition of

213 neutralisation buffer (40 mM Tris-HCl, pH 5). The PCR reaction was performed through
214 addition of MyTaq DNA Polymerase (Bioline) reaction buffer and primer pairs:
215
216 TAS (APP_{Swe}):
217 5' GAATTGACAAGTTCCGAGGG 3'
218 5' GGGTACTGGCTGCTGTTGTAG 3'
219
220 TPM ($PSEN1_{M146V}$):
221 5' GTTACCTGCACCGTTGTCCT 3'
222 5' GCTCCTGCCGTTCTCTATTG 3'
223
224 using the cycling parameters: 94°C (30 s), 58°C (30 s), 72°C (30 s), for 30 cycles and a
225 final extension at 72°C for 4 min. PCR product sizes 366 bp for TAS and 104 bp for TPM.
226
227 **Immunohistochemistry**
228 Animals were deeply anaesthetised (1:10 Euthatal:Intra-Epicaine, National Veterinary
229 Supplies) and transcardially perfused with 0·1 M phosphate buffer saline (PBS) followed
230 by 10% buffered formal saline (Pioneer Research Chemicals Ltd). Alternatively, single
231 hemispheres were drop-fixed immediately following brain extraction for
232 electrophysiology. The brains were post-fixed in 10% buffered formal saline for 24hrs
233 and cryoprotected in 30% sucrose/0·03% sodium azide/PBS at 4°C for at least 24hrs
234 before sectioning or storage. Transverse sections were cut at 30 μm through the full left
235 hippocampus using a frozen sledge microtome (SM 2000 R, Leica) and collected into a
236 24-well plate containing PBS/sodium azide (0·03%) for storage at 4°C. Serial sections
237 were placed in separate wells until all wells contained a section and collection then
238 continued serially from Well 1 so that within each well the transverse sections were
239 from the length of the hippocampus at least 720μm apart.
240
241 Standard immunohistochemical techniques were employed. For Aβ staining only,
242 antigen retrieval was achieved by submerging sections in 10 mM sodium citrate (pH 6·0)
243 in 0·05% Triton X-100 and heated in a water bath at 80°C for 30 minutes. Sections for all
244 immunohistochistry were then washed in PBS, followed by 0·3% Triton X-100 in PBS
245 and subsequent blocking in 8% horse serum/Triton/PBS for 1 hour. Incubation with

246 primary antibody (table 1) in blocking solution was performed overnight at 4°C.
247 Sections were again washed with Triton/PBS. The appropriate Alexa-conjugated
248 secondary antibody (1:500; Invitrogen) was added to blocking solution for a 2-hour
249 incubation at room temperature in the dark. Following PBS wash, DAPI (1:10,000) was
250 applied to all sections for 5 minutes. Sections were washed for a final time in PBS before
251 mounting. Age-matched sections from wild type controls were stained in parallel for all
252 ages. Sections were mounted in anatomical order onto SuperFrost Plus glass slides by
253 floating on PBS and then cover-slipped using Fluoromount G mounting medium.
254
255 *Imaging and data analysis*
256 Sections were imaged for quantification using an EVOS FL Auto Cell Imaging System
257 (Life technologies). Tiled images were taken of the whole transverse hippocampal
258 section using a 20X objective. To determine cell densities, an area of 400 μm x 240 μm
259 was defined in the CA1, CA3 and the inner blade of the dentate gyrus. Cell counts were
260 performed using Adobe Photoshop CS6. A minimum of three sections were used to
261 create a mean for each animal. Sections for any given condition were obtained from the
262 same collection well within the 24-well plate and were therefore a minimum of 720 μm
263 apart, thus avoiding multiple counts of the same cells. Counts of objects touching the
264 boundaries of the area of interests were only included from the north and east borders
265 and excluded from the south and west borders.
266
267 **Electrophysiological recordings**
268 *Acute hippocampal brain slice preparation*
269 Mice were decapitated and the brain rapidly removed and placed in ice-cold dissection
270 artificial cerebrospinal fluid (ACSF, containing (in mM): 125 NaCl, 2·4 KCl, 26 $NaHCO_3$,
271 1·4 NaH_2PO_4, 20 D-glucose, 3 $MgCl_2$, 0.5 $CaCl_2$, pH 7·4, ~315 mOsm/l). After
272 approximately two minutes in ice-cold dissection ACSF, the brain was prepared for
273 slicing by removing the cerebellum, hemisection of the forebrain and a segment cut
274 away from the dorsal aspect of each hemisphere at an angle of approximately 110° from
275 the midline surface to optimise slicing transverse to the hippocampus. Each hemisphere
276 was then glued with cyanoacrylate (Loctite 406, Henkel Loctite Limited, UK) on this
277 surface onto the stage of a vibrating microtome (Integraslice model 7550 MM, Campden
278 Instruments, Loughborough, UK) containing frozen dissection ACSF and 400 μm

transverse slices of hippocampus cut. As each slice of a hemisphere was cut, the hippocampus was dissected out, retaining a portion of entorhinal cortex and the resulting smaller slice was placed into a chamber containing 'Carbogenated' (95% O_2/5% CO_2; BOC Limited) dissection ACSF at room temperature (approximately 21°C). After 5 minutes, slices were then transferred into a fresh chamber held at 36°C with the same dissection ACSF. At 5-minute intervals, they were then consecutively transferred to physiological Ca^{2+} and Mg^{2+} ion concentrations (in mM): i) 1 Mg^{2+}, 0.5 Ca^{2+}; ii) 1 Mg^{2+}, 1 Ca^{2+}; iii) 1Mg^{2+}, 2 Ca^{2+}. After approximately 20 minutes at 35°C (i.e., once transferred into the 1 Mg^{2+}, 2 Ca^{2+} ACSF).

Patch-clamp recordings in brain slices

Once transferred to 1 Mg^{2+}, 2 Ca^{2+} ACSF, slices were allowed to return to room temperature and after at least a further 40 minutes recovery time, a single slice was transferred to a submerged chamber and superfused with recording ACSF (containing (in mM): 125 NaCl, 2·4 KCl, 26 $NaHCO_3$, 1·4 NaH_2PO_4, 20 D-glucose, 1 $MgCl_2$, 2 $CaCl_2$, bubbled with Carbogen). Individual CA1 pyramidal or dentate gyrus granule neurones were visualised using infrared-differential interference contrast microscopy on an upright microscope (model BX50WI, Olympus, UK). Glass microelectrodes for patch-clamp were pulled from borosilicate glass capillaries (Catalogue number GC150F-7.5, 1·5 mm OD x 0·86 mm ID, Biochrom-Harvard Apparatus Ltd, Cambridge, UK) on a vertical puller (model PP830, Narishige International Ltd, London UK). Electrodes (tip resistance approximately 5 MΩ) were filled with a CsCl-based internal solution (containing (in mM): CsCl 140, HEPES 5, EGTA 10, Mg-ATP 2, pH 7·4, ~290 mOsm/l). Patch-clamp recordings were performed using an Axopatch 1D (Molecular Devices, Sunyvale, CA, USA), and current signals low-pass filtered at 10 kHz then 2 kHz (Brownlee Precision Model 440, NeuroPhase, Santa Clara, CA, USA) during digitization (10 kHz; 1401plus, Cambridge Electronic Design, Limited, Cambridge, UK) and acquired using WinWCP (for isolated events; version 4.6.1; John Dempster, Strathclyde University, UK) and WinEDR (for continuous recordings; John Dempster, Strathclyde University, UK). Stimulation was applied *via* a patch electrode filled with ACSF, placed extracellularly in the appropriate axon path using a square pulse constant-voltage stimulator (100 µs; DS2A-MkII, Digitimer Ltd, UK) triggered by WinWCP.

312 WinEDR synaptic analysis software was used for detection of spontaneous and
313 miniature currents and WinWCP used to analyse identified spontaneous, miniature and
314 evoked currents. Criteria for detection of spontaneous or miniature currents was to
315 remain over a threshold of 3 pA for 2 ms. Currents were inspected by eye and only
316 included if the rise time was <3 ms and faster than the decay.
317
318 *Field potential recordings in brain slices*
319 Slices were transferred as needed to a heated (30±1°C) submerged chamber and
320 superfused with ACSF and allowed to recover for 1 h in the recording chamber. A glass
321 stimulating electrode (filled with ACSF, resistance ~2 MΩ) and an identical recording
322 electrode (connected to an AxoClamp 1B via a 1X gain headstage) were both positioned
323 in stratum radiatum of the CA1 field to obtain a dendritic excitatory postsynaptic field
324 potential (fEPSP). Recordings were controlled and recorded using WinWCP software (as
325 above), filtered at 10 kHz and subsequently at 3 kHz and digitized at 10 kHz via a
326 micro1401 interface (Cambridge Electrical Designs, UK). Stimuli (constant voltage 10-
327 70V, 100 μs; model Digitimer DS2A-MkII or Grass SD9) were applied at 0·1 Hz and
328 resultant fEPSPs subsequently averaged over consecutive 1-minute intervals.
329 Stimulation intensity was set at approximately 30-50% of the intensity required to
330 evoke a population spike or the maximum fEPSP amplitude obtained and a ≥15-minute
331 stable baseline recorded. LTP conditioning was applied at test-pulse stimulus intensity
332 and consisted of either 3 trains of tetani, each consisting of 20 pulses at 100 Hz, 1·5 s
333 inter-train interval or 4 trains of theta-burst stimuli (TBS), each train consisting of 4
334 pulses at 100 Hz repeated 8 times at 20 Hz; inter-train interval 1 minute. Following
335 conditioning, fEPSPs were evoked at 0·1 Hz for 1 hour.
336
337 **Behavioural testing**
338 *T-maze forced alternation task*
339 Previously reported methods, optimised for mouse, were used to assess hippocampus-
340 dependent learning [18]. Mice were food deprived to 90% free-feeding-weight, beginning
341 2 days before the start of the habituation phase and with *ad libitum* access to water.
342 Each mouse was handled at the start of food deprivation and throughout T-maze
343 habituation for 15-20 minutes per weekday.
344

The T-maze was constructed from three arms, each measuring 50 x 8 cm with 10 cm colourless Perspex walls and a grey floor, mounted on a table in the centre of a room with numerous distal visual cues, such as black and white posters on the walls. Black barriers were used to block the start and goal arms. Reward consisted of a drop of Nestlé Carnation™ condensed milk that was placed at the end of each goal arm. Arms were cleaned with 70% ethanol between all runs to reduce odour cues. In addition, in an inaccessible well a drop of reward is always present in both arms.

Mice received 4 days of habituation to the maze, during which time they were allowed to explore the maze for 5 minutes with all arms open. During the first two days of habituation, reward was scattered along the floor and in food wells to encourage exploratory behaviour; then restricted to only the food wells at the ends of the goal arms in the last two days.

The behavioural regime lasted for three weeks, with five days of training per week. Each day, animals received six trials; each trial consisted of a sample and choice run. In the sample run, one arm was blocked off. The mouse was placed at the starting point at the base of the T, the barrier was removed and the mouse was allowed to go to the available arm and given 20 s to eat a drop of reward from the food well. For the choice run, the mouse was immediately returned to the starting point and the barrier in the previously blocked arm removed. The starting barrier was then raised and the animal allowed to choose between the two arms but only rewarded if it chose the previously unvisited arm. Thus, a correct choice was scored when the mouse selected the arm not visited in the sample run. After the choice run, the mouse was removed from the maze and placed in its holding box. The location of the sample arm (left or right) was varied pseudorandomly across the session and mice received three left and three right presentations, with no more than two consecutive trials with the same sample location. Animals were allowed a maximum of 5 minutes to make a choice to enter a goal arm in both runs before a trial was aborted. If an incorrect arm was chosen during the choice run, the mouse was confined in the arm with no reward for 20 s and then removed from the maze.

During the first two weeks of training the choice run followed immediately after the sample (test) run (there was a delay of approximately 15 s between runs for cleaning and resetting the maze). Data was analysed in blocks of 2 days and hence blocks 1-5 represent the first 2 weeks of training.

On the first day of the third week, mice received a repeat of the previous training sessions in order to assess retention of the task (block 6). On the following four days, longer delays (2-10 minutes) were introduced between the sample and choice runs to extend the time that the previous choice was to be held in memory (blocks 7 and 8 in response times). During these intervals, each animal was placed in a separate holding box. Each mouse received two of each of the delay periods per day, varied pseudorandomly both within and across days. Response times were calculated from the time that the starting block was removed until the mouse made a choice of arms and all four paws had crossed the entry point. Squads of 15-17 mice were run per day. During training data are presented as blocks averaged across 2 days for each animal and expressed as mean ± SEM. For delays the four runs for each delay are averaged.

Elevated plus maze

The plus-maze was constructed from two enclosed arms (30 cm x 5 cm x 20 cm) and two open arms (30 cm x 5 cm x 0.8 cm) connected by a small central platform (5 x 6 cm); the two closed and two open arms were positioned opposite each other, respectively. The maze was elevated 30 cm above a table.

Mice were placed in the centre of the plus maze facing an open arm and allowed to freely explore the maze for one 6-minute trial. The time spent on each arm (open *versus* closed) was recorded, as well as the number of entries into the arms. An entry into an arm was defined as all four paws resting on a given arm.

Open field

The open field consisted of a plastic cylinder (diameter: 47·5 cm, height 36 cm) with a white plastic floor. Mice were placed on the periphery of the open field floor and allowed to explore freely for 30 minutes. The path of each mouse was recorded using dacQUSB recording system (Axona, St. Albans, U.K) at a sample rate of 50 Hz. The open field was

optically divided into a central circle and a peripheral ring, each with equal area. The path of the mouse was analysed offline using ImageProPlus. Path length and dwell times in the periphery and centre were calculated using custom made routines written in Matlab R2010a (MathWorks).

Light/dark box

The dark box[19] measured 20 cm x 20 cm x 30 cm, with black walls, floor and lid. The light box measured 30 cm x 30 cm x 30 cm with a white floor and light grey walls. The boxes were connected by an opening in the partition between the two compartments. An overhead light provided bright illumination in the light box. Mice were placed in the centre of the light compartment facing away from the opening and then allowed to explore for a period of 6 minutes. Time spent in each box and the number of entries into each box were recorded. An entry into a box was defined as all four paws resting inside the given box.

Statistics

All data analysis was carried out blind to genotype. All statistics were performed using Graphpad Prism 6 with appropriately designed two-tailed t-test or ANOVA. Post hoc tests were only performed if a significant interaction between the independent variables was obtained. Animals were considered as independent samples and, where multiple data were collected from an animal, these were averaged (mean) prior to pooling. Thus sample sizes represent the number of animals. Unless stated otherwise, data are presented as mean ± SEM and differences considered significant at $p<0{\cdot}05$.

433 **Results**

434 *Plaque development in hippocampus*

435 In TASTPM mice of different ages, individual plaques were counted in the hippocampus
436 and their sizes measured to assess whether the distribution changed over time (Fig 1).
437 Initially, at 3-4 months of age, only small plaques could be detected (<100 μm^2) and
438 these were very sparse (Fig. 1a-c). However, the number of small plaques increased
439 exponentially, initially approximately doubling every month, and continuing to increase
440 at a slower rate until 14 months of age (Fig. 1b). Hence, at least up until this age, new
441 plaques were being seeded. By 7 months plaques up to 200 μm^2 were consistently seen
442 but were similar in frequency to the smallest plaques at 3-4 months, presumably
443 representing the growth of the earliest seeds. Plaques of >500 μm^2 were only
444 consistently detected at ages over 10 months but, from this age on, a wide range of
445 plaques sizes were evident, with occasional plaques of over 2500 μm^2 detected.
446 Interestingly, between 14 and 15 months of age, very little change in the number of
447 plaques was detected but the largest plaques continued to grow. As individual plaques
448 were not tracked over time, we cannot be entirely sure that the progression up to 14
449 months is due to continuous seeding of small plaques that gradually grow with ongoing
450 plaque deposition; however, this seems the most likely explanation. The fact that the
451 rate of addition of small plaques decreases gradually until it plateaus around 14 months
452 of age suggests that, as the plaques get denser, some of the small plaques start to fuse
453 with larger plaques. In some cases, large plaques were present that possessed a halo of
454 Aβ around the dense core, with dense puncta of Aβ visible within the halo, possibly
455 representing more recently seeded plaques being engulfed as the large plaque grows
456 (Fig 1a).
457
458 When the gene-dose was doubled by using double homozygous TASTPM mice, plaques
459 were first detected at about 2 months of age (Fig 1e). Similarly to the hemizygous mice,
460 plaque density and size increased with age but perhaps surprisingly, did not reach a
461 greater density than that observed in the hemizygotes.
462
463 Mice carrying only the single mutations were also examined. In TAS mice (APP_{Swe}), small
464 plaques were detected at 16 months. While plaque density and size increased with age,
465 plaque loads did not reach that seen in the double mutant TASTPM mice, even at the

466 very advanced age of 27 months. In TPM mice ($PSEN1_{M146V}$), there were no plaques
467 observed at any age.
468
469 *Microglia*
470 Having previously observed that a module of microglial genes increased in expression in
471 Aβ mice (including TASTPM) in close correlation with plaque load[10], we went on to
472 examine the densities of total and CD68 positive of microglia in more detail in these
473 mice (Fig 2). There was an increased density of microglia (assessed by Iba1 positive
474 cells) in CA1 at very early ages, with increases (approximately double) compared to wild
475 type already evident by 2 months of age, even before plaques could be detected (Fig
476 2a&c; 2-8 months, n=6-12, two-way ANOVA, $p<0{\cdot}01$). However, note that Aβ levels are
477 already raised by 2 months[16] and it is possible that small plaque seeds (< the 10 μm^2
478 threshold) may already be depositing at this time. There was also an age-dependent
479 increase in Iba1 positive microglia in both wild type and TASTPM mice at around 10
480 months of age.
481
482 In contrast to total microglia, the microglial phagocytic phenotype, as measured by CD68
483 labelling, was very low in all young animals and only increased from around 10-12
484 months. Again, this happened in both wild type and TASTPM mice. The percentage of
485 phagocytic microglia tended to be slightly higher in TASTPM mice as compared to wild
486 type (14-20 months, n=5-9, two-way ANOVA $p=0{\cdot}07$). This coincided with the
487 appearance of large plaques (Fig 1c&d). Interestingly, the number of microglia and their
488 CD68 status seem to plateau at this stage, with no further increase in density beyond 12
489 months of age.
490
491 When the double homozygous TASTPM mice were examined, a very similar pattern was
492 observed for densities of both total microglia and CD68 positive microglia (Fig 2d). As
493 expected both plaque load and microglial response was greater in the homozygous mice.
494
495 Sections from single mutant mice were also stained for both IBA1 and CD68. The APP_{Swe}
496 TAS mice, which develop plaques from around 16 months (Fig 1f), had a higher total and
497 CD68 positive microglia at both 18 and 27 months of age (main effects of genotype for
498 both Iba1 and CD68 in separate two-way ANOVAs; $p<0.05$). In contrast, the $PSEN1_{M146V}$

TPM mice, which do not develop plaques at any age, showed no difference from wild type mice in their microglial phenotype at 4 months of age for either total or CD68 positive microglia (Fig 2g, two-tailed t-test, $p>0.5$).

Very similar changes in total microglial and CD68 positive microglial densities were found in dentate gyrus, CA3 and subiculum (data not shown).

Synaptic currents in CA1 neurones

Spontaneous excitatory activity

When spontaneous excitatory currents are recorded from CA1 pyramidal neurones in the presence of a $GABA_A$ receptor antagonist (gabazine, 6 μM), the substantial loss of spontaneous activity we have previously reported up to 4 months of age[16] is largely maintained through to 18 months (Fig 3a). At 8 months there was almost a complete loss of action potential-dependent spontaneous activity in the transgenic mice (Fig 3aii), with the frequency almost exactly the same as that of miniature currents (Fig 3aiii) observed in the presence of 1 μM tetrodotoxin. This result was almost identical to what we have previously reported at 4 months. By 12-18 months, a decrement in frequency of miniature EPSCs had also developed but the action potential mediated spontaneous excitatory current frequency, although significantly lower in transgenic mice than wild type mice, were at a higher frequency than the miniature currents in the same genotype, implying that some spontaneous action potential-mediated activity was occurring in the transgenic mice at these older ages (Fig 3a). There were no differences between genotypes of mEPSC amplitudes or decay time constants (data not shown).

When excitatory activity was evoked by stimulating the Schaffer collaterals in slices from older animals, the previously reported increase in release probability at 4 months, as assessed by a lower paired-pulse facilitation and confirmed by a reduction in failure to release glutamate in response to minimal stimulation[16], was maintained. Thus, at 12 months of age, paired-pulse ratio was lower in TASTPM than wild type mice at both 25 and 50 ms inter-stimulus intervals (n=5-8, two-way ANOVA, main effect of genotype $p<0{\cdot}02$), while at 18 months of age, the lower paired-pulse ratio was only evident at 25 ms, resulting in a genotype x interval interaction ($p<0{\cdot}05$) and a highly significant Sidak post hoc pairwise comparison between genotype at 25 ms ($p<0{\cdot}005$).

532

533 Inhibitory activity is unchanged

534 Although we have concentrated our detailed analysis on glutamatergic activity, we were
535 able to gain an overview of inhibitory activity from the spontaneous activity recorded in
536 the absence of antagonists by utilising CsCl as the internal patch pipette solution. Hence,
537 in the experiments examining pharmacologically isolated EPSCs above, initially
538 spontaneous currents were recorded in the absence of receptor antagonists. When the
539 $GABA_A$ receptor antagonist was included in the perfusion solution, the frequency of
540 currents was decreased to about 5-10% in wild type slices. Consequently, $GABA_A$
541 receptor-mediated activity contributes about 90% of the frequency of the initial
542 recording of mixed spontaneous activity. Note that, if the recording were made in the
543 presence of a glutamatergic antagonist, any currents that were due to spontaneous
544 glutamatergic activity mediating feed-forward or feed-back inhibition would be lost.
545 Hence, the assessment of the drug-free frequency is a better assessment of the
546 contribution of inhibition with the understanding that this will overestimate frequency
547 by about 10%. Under these conditions we find that there is no significant change in
548 inhibitory synaptic activity in TASTPM mice at any age from 4 to 18 months (Fig
549 3c). Note that, considering the very substantial change in spontaneous glutamatergic
550 activity, this implies that very little of the GABAergic activity is dependent on
551 glutamatergic input.

552

553 Synaptic plasticity is altered in TASTPM mice

554 Considering the changes in excitatory transmission it seemed likely that synaptic
555 plasticity, in particular, long-term potentiation (LTP), the best cellular model we have
556 for the laying down and retrieval of memory[20], could be altered. To assess effects on
557 LTP, field potentials were recorded from CA3-CA1 synapses in acute brain slices
558 prepared from TASTPM mice at ages preceding detectable Aβ plaques (2 months)
559 through to ages with a heavy plaque load (12-18 months).

560

561 Field input-output relationship was not significantly changed at any of the ages tested
562 (Fig 4a). Moreover, unlike our previously reported result using patch clamp recording in
563 the presence of a $GABA_A$ receptor antagonist[16], in field recordings with the inhibitory
564 network intact, paired-pulse ratios were not significantly changed between genotypes at

565 any of the ages tested (Fig 4b). This suggests that the observed changes in paired-pulse
566 ratio were masked when GABAergic activity was not blocked, presumably, at least in
567 part, by feed-forward inhibition decreasing release on the second stimulus.
568
569 At 2 months of age, LTP is altered in TASTPM mice but this is dependent on the
570 induction protocol. When LTP was induced by tetanic stimulation in these young mice,
571 the magnitude of LTP was greater in slices from TASTPM than from wild type mice.
572 Paired-pulse ratios remained unaltered when the last ten minutes of the post-induction
573 recordings was compared to the baseline in both genotypes (Fig 4c&d). This suggested
574 that the change in amplitude seen in LTP was due to a postsynaptic change. In contrast,
575 when LTP was induced using TBS, there was no difference between the wild type and
576 transgenic mice (Fig 4e). Surprisingly, however, despite LTP remaining unchanged after
577 theta burst stimulation, the paired-pulse ratio decreased significantly between the pre-
578 induction baseline and the last 10 minutes of LTP in the TASTPM but not in the wild type
579 mice. This suggests that the locus of expression of this form of LTP is likely to have a
580 presynaptic component in transgenic mice at this age. Note that, considering an increase
581 in release probability would be expected to enhance the postsynaptic response, this
582 would suggest that the postsynaptic contribution to LTP could be decreased in the
583 transgenic mice possibly with one locus of change compensating for the other.
584
585 At 4 months of age, the effects of the different stimulus protocols had changed. By this
586 age, a clear deficit was seen in LTP induced by tetanic stimulation, which was the
587 reverse change to that seen at 2 months. Moreover, similar effects were seen in two
588 separate cohorts of 4-month-old mice (cohort 1 shown in Fig 4c; pooled data shown in
589 Fig 4d.
590
591 TBS-induced LTP (Fig 4e) was, like at 2 months, of similar magnitude between
592 genotypes but analysis of paired-pulse ratios, following LTP induction, indicated that
593 LTP has a similar locus of expression in the two genotypes.
594
595 In addition, chemically-induced LTP was also examined in a separate set of slices, using
596 transient application of the potassium channel blocker tetraethylammonium, applied
597 after completion of a tetanus-induced LTP experiment. As expected,

598 tetraethylammonium application resulted in an initial reduction in the field potential,
599 followed by a long-lasting increase after wash-out. The magnitude of the
600 tetraethylammonium-induced LTP was unchanged in slices of TASTPM compared to
601 wild type animals (data not shown). This confirms that, despite deficits in tetanus-
602 induced LTP, TASTPM are capable of expressing LTP under other induction protocols.
603
604 The deficit in tetanus-induced LTP was maintained at 12 and 18 months of age (Fig 4e).
605
606 Synaptic plasticity in TAS and TPM mice
607 The induction of LTP was also examined in 24 month old single mutant mice (Fig 4f-h).
608 In age-matched wild type mice, LTP magnitude was similar to that observed at younger
609 ages. In the APP_{Swe} TAS mice, the magnitude of LTP was smaller than wild type mice (Fig
610 4f). In contrast, in the $PSEN1_{M146V}$ TPM mice, the magnitude of LTP was greater (Fig 4g).
611 There was an overall significance between genotypes by one-way ANOVA ($p<0.05$; Fig
612 4h, Fisher LSD *post hoc* tests versus wild type $p=0.1$ for TAS and $p=0.05$ for TPM).
613
614 *Cognition and behaviour*
615 TASTPM mice show rigidity in hippocampus-dependent learning
616 The hippocampus-dependent forced-alternation T-maze task was used to assess
617 cognition in the TASTPM mice at three ages (Fig 5): 4 months, which corresponds to the
618 first appearance of Aβ plaques (Fig 1) and where tetanus induced LTP was first impaired
619 (Fig 4); 8 months, a moderate plaque load and 12 months, a heavy plaque load. Due to
620 availability of animals, in this set of experiments, the 4-month-old group was run as
621 three cohorts (no significant difference between the cohorts); while the 8- and 12-
622 month-old group were a single cohort that underwent repeat training in a longitudinal
623 study. It should be noted that at both 4 and 8 months of age, a subset of TASTPM mice
624 did not complete the task in the required time and these mice were not included in the
625 final results (1 of 16 mice at 4 months of age and 3 of 13 mice at 8 months of age).
626
627 At 4 months of age, both genotypes started training at similar levels of performance and
628 improved over the training period (Fig 5a, two-way ANOVA, main effect of 5 block
629 training period, $p=0{\cdot}01$). However, TASTPM performed significantly worse than wild
630 type mice overall (main effect of genotype, $p<0{\cdot}003$), and there was no significant

interaction between training block and genotype. Interestingly in Block 6, after 2 days without training, the two groups came together with almost identical performance at 90% correct choices (Fig 5a). When extra delays (2-6 minutes) were then added between the sample and choice runs a slight decrement in performance occurred, as expected, but there was no difference between genotypes (Fig 5b). In terms of the behaviour within the trials it was notable that on both the sample and choice runs the TASTPM mice showed considerably longer response times. In the case of the choice run, this may have influenced the result, especially the apparent impairment during the training period, as the time that memory needed to be retained was more than doubled (Fig 5c).

At 8 months of age, TASTPM performed similarly to wild type mice, improving over the training period (two-way ANOVA, main effect of training period ($p<0{\cdot}0001$). When the same mice that were run at 8 months were retested at 12 months of age, wild types had, as expected, returned to the baseline response of approximately 75% correct and again improved from ~75% to ~90% during the training period. Unexpectedly however, TASTPM appeared to have retained their previous training, starting the training at ~90% and showed no further improvement over the training period. This was reflected in a significant interaction between training period and genotype in a two-way ANOVA ($p<0{\cdot}03$, Fig 5a).

Animals were again challenged further by the introduction of a delay between sample and choice runs (Fig 5c). While at 8 months there was no difference between genotypes, at 12 months of age although TASTPM mice showed a similar decrement with the longest delays their performance with a 2·5 minute delay between sample and choice runs was surprisingly better than their wild type counterparts (two-tailed t-test, $p<0{\cdot}05$).

Another interesting difference between the 12-month mice and the younger groups was that the response time for the choice run for TASTPM mice at 12 months was rapid and no different from the wild type mice (Fig 5c). (Note, at this age the mice also always completed the task in the required time.) In contrast, as described for 4 months above, the 8-month-old TASTPM mice showed a considerable delay to respond. However,

despite this delay again increasing the time that memory needed to be retained, the 8 months mice showed no decrement in correct choices.

These failures and delays to respond may be interesting in terms of early behavioural changes and may also suggest different levels of anxiety.

<u>TASTPM mice show decreased activity and increased anxiety-related behaviour compared to wild type mice.</u>

In the light of the behavioural differences seen in the T-maze trials, locomotor activity and anxiety were assessed using a battery of tests. First, mice were placed in an open field (Fig 6a). TASTPM mice had shorter total path lengths than their wild type counterparts at all ages (Fig. 6ai; two-way ANOVA, main effect of genotype, $p<0{\cdot}0001$; no interaction between age and genotype). Furthermore, TASTPM mice spent more time in the peripheral than central area (Fig. 6aii; two-way ANOVA, main effect of genotype, $p<0{\cdot}0005$; main effect of age, $p<0{\cdot}0001$).

Secondly, at 8 months of age, TASTPM mice spend more time in the closed than open arms of an elevated plus maze (two-way ANOVA interaction between age and genotype $p<0{\cdot}05$); at 4 and 12 months of age this difference was not evident (Fig. 6b).

Finally, at 4 and 8 months of age, TASTPM mice spent more time in the closed compartment of a light/dark box (12 months not tested). There was a significant interaction between age and genotype (Fig. 6c; $p<0{\cdot}05$).

Overall, these data indicate an increased level of anxiety in TASTPM mice from early stages of plaque development especially at earlier ages.

690 **Discussion**

691 *Pathology and microglia*

692 Proliferation of microglia, particularly clustering around plaques, has been repeatedly
693 reported in Alzheimer's disease, both in the human condition and in mouse models.[21-23]
694 Moreover we have previously reported a close correlation between plaque load and a
695 microglial coexpression module in TASTPM mice. This reveals not only changes in
696 expression of the gene for the phagocytic protein CD68, tested with
697 immunohistochemistry in the present study but also even greater changes in *Trem2*
698 expression,[10] a gene shown in humans to be important in Alzheimer's disease in
699 GWAS.[24, 25] However, here we show increased density of microglia, even before plaques
700 can be detected in this mouse model. This finding required immunohistochemistry and
701 cell counts as the gene expression changes of such specific microglial genes would only
702 be apparent in whole tissue analysis with very large changes, such as occurs in later
703 stages. In the light of previous reports,[21-23] proliferation seems the most likely
704 explanation of the increased density, although other causes such as increased survival of
705 microglia or migration into the hippocampus, are possible. The triggering of microglial
706 proliferation may be due to soluble Aβ in the wider neuropil, as seem to be the case for
707 the earliest synaptic changes.[16] Alternatively, it is possible that initial seeds of plaques
708 are already present at this early stage but are too small to detect, being below the
709 detection threshold set here (<10 μm^2).

710

711 In either case, the question arises as to how plaque development then continues and
712 how this relates to increased microglial numbers and development of a reactive
713 phagocytic phenotype. Once plaques are seeded at these early stages, the ongoing
714 deposition may primarily contribute either to the growth of plaques or to the seeding of
715 new plaques. It is also possible that large plaques are not the result of smaller plaques
716 growing but rather due to the fusion of smaller plaques. Here we observe that the
717 smallest plaques initially increase in number, almost doubling each month. This rate
718 continues to increase, albeit not quite so rapidly, at least until about 14 months of age
719 when the number of plaques plateaus. This suggests that small plaques are seeded
720 throughout the ages tested and gradually grow to form the larger plaques. Presumably
721 the rapid increase in the seeding of plaques during the early stages relates to the rapid
722 increase in Aβ levels at this stage that we have previously reported.[16] The plateauing of

723 density of smaller plaques may also reflect them being gradually being engulfed as the
724 larger plaques spread and thus they are no longer seen as separate entities. This is
725 strongly suggested by the appearance of brighter spots of Aβ in the halo around some of
726 the larger plaques as can be seen in Fig 1a from 10 months onwards.
727
728 As plaques form, we have previously shown a very strong correlation with microglial
729 gene expression.[10] This encompasses both proliferation and activation of microglia.
730 While there are more microglia very early in these Aβ mice, their phagocytic phenotype
731 appears later and seems only to be triggered once the larger plaques of >500 μm^2
732 develop. However, it is important to note that a step up in the density of total and CD68
733 positive microglia also occur at this stage in the wild type mice. Although the number of
734 microglia and their activation state remains higher in the TASTPM mice the similarity in
735 the timing of this later stage in both genotypes suggests that this has a strong age-
736 related component rather than being purely dependent on the presence of plaques.
737 However, it is also interesting to note that in the homozygous TASTPM, which develop
738 plaques earlier but plaque load plateaus at the same level as the hemizygous mice, the
739 density of total microglia and CD68 positive microglia is higher than in hemizygotes.
740 Furthermore, the absence of a microglial phenotype in the TPM mice, while the TAS mice
741 show a similar phenotype excludes a direct effect of the mutant presenilin on microglial
742 function.
743
744 As has been previously shown in TASTPM[10] and other transgenic mice (for example,
745 see reference 22), the microglia are strongly attracted to and cluster tightly around the
746 plaques as they grow. The question arises as to what the microglia are actually doing in
747 the Aβ mice. The assumption previously has been that they are removing or limiting
748 expansion of plaques.[22] Conversely, it has been repeatedly reported that removal of
749 microglia by blocking CSF1R has no effect on plaque load,[26-28] although a role for
750 microglia in initial plaque deposition has been suggested,[29] which may be related to the
751 initial early rise in microglia numbers, even preceding detection of plaques. It is,
752 however, clear in the TASTPM mice that, since plaques continue to grow in both size and
753 number in parallel to rapid microglial proliferation, it does not seem that microglia are
754 very effective at removing Aβ. Recently interesting evidence has been presented that Aβ
755 stimulates microglia to phagocytose synapses in a complement dependent manner at

early stages of plaque development in J20 ($APP_{Swe/Ind}$) mice[30] leading to the hypothesis that microglia are causing early synaptic damage. We put forward an alternative hypothesis that the microglia are rather removing spines and boutons damaged by the high levels of soluble Aβ in or near the plaques and that this may represent a protective function, avoiding further damage to the dendrites and axons affected and hence protecting network function. This is further supported by the observation that as plaques grow synaptic loss is concentrated near to the plaques and the loss decreases further from plaques.[31, 32]

Synaptic transmission

At 8 months of age the synaptic changes observed are almost identical to those we have previously reported at 4 months, with no change in miniature currents but a complete loss of spontaneous activity and an increase in release probability of glutamate. Particularly at early stages, the plaque load in terms of the percentage tissue coverage is very low and so very few of the synapses recorded would be close to a plaque. Moreover, the observation that the change in paired-pulse ratio is similar despite a rising plaque load also suggests that the plaques themselves are unlikely to be causing this effect. Hence, this is presumably the result of very low levels of soluble Aβ throughout the tissue. Increased release probability has been reported to be the physiological effect of Aβ release in wild type rats.[5] As the plaque load increases and larger plaques start to appear, additional changes become evident. At 12 months, although the evoked release probability is still similarly affected, being higher in the transgenic mice than the wild type mice, there is also a reduction in the frequency of miniature EPSCs. The simplest interpretations of loss of miniature frequency is either a loss of functional synapses or a decreased release probability (see reference 33 for review). As we have demonstrated that release probability is increased, this suggests that there is a loss synapses is the likely explanation. In and around the plaques soluble and insoluble Aβ will be in equilibrium and with increased plaque coverage with age, at least some of the synapses will be directly affected by the high local concentration of Aβ in the close vicinity of a plaque which could lead to this loss. Note that unlike evoked currents, miniature synaptic currents can originate from any synapse in the tissue and hence some will be physically near plaques. The increasing effect as the plaque load rises, supports this hypothesis. This is again consistent with the observation that synaptic loss occurs with

increased plaque load but that the loss is inversely proportional to distance from a plaque.[31]

It is notable that the decrease in frequency of miniature EPSCs observed at 12 months coincides with the increase in microglial number and activation but that it does not decrease any further by 18 months. This is consistent with the plaque load and indeed the microglial density largely plateauing by 14 months. The very effective microglial proliferation and subsequent phagocytic phenotype, associated with strong upregulation of microglial genes such as *Trem2* that we have previously reported at this age,[10] may be one of the reasons why the progression of Alzheimer's pathology to neurofibrillary tangles and neurodegeneration does not go further in these mice.

Synaptic plasticity

The biphasic change in LTP induced by a mild tetanic stimulus at the early stages of pathology in Aβ mice is of interest. At 2 months of age, prior to detection of plaques, when LTP is enhanced in the Aβ mice, Aβ is certainly present, albeit at low levels.[10, 16] By 4 months of age, when the first plaques are evident, Aβ levels are at least 10-fold higher than at 2 months. At this stage the opposite effect is observed with magnitude of tetanus-induced LTP much reduced compared to wild types. This LTP deficit was maintained both at 12 and 18 months of age. The biphasic pattern of change may reflect the increasing glutamate release probability which we have previously shown is greater at 4 months than at 2 months of age. If glutamate were more readily released during conditioning, the initial outcome may be a greater calcium influx through NMDA receptors and thus a larger magnitude LTP. However, as levels rise by 4 months and release probability increases further, depletion of the readily-releasable pool of synaptic vesicles during the first pulses of the conditioning train may result in a failure to release transmitter as the train continues, thus impairing LTP. Alternatively, the higher levels of Aβ may have other effects, interacting with NMDA receptors directly and impeding LTP (reviewed in reference 34). Moreover, Aβ is itself proposed to be released in an activity-dependent manner[35-37] and hence, as its levels rise, resulting in increased release probability, this could lead to a positive feedback.

In concert with (or alternatively to) the direct physiological effects of low levels of Aβ, the early increase in LTP magnitude we report could be an interaction with the mutant presenilin 1. Expression of both normal and mutant presenilin 1 has direct effects on synaptic transmission and plasticity. For example, the A246E mutation leads to increased LTP magnitude at young ages,[38, 39] while the L286V mutation increases LTP magnitude at young ages but decreases at older (14 month) ages.[40] Here we show that the M146V mutation increases the magnitude of LTP at 24 months of age, which could be the underlying mechanism of the initial increased LTP observed in the TASTPM, until the later Aβ effects become dominant, decrementing the LTP.

Interestingly when theta burst stimulation was used for induction, during which the readily-releasable pool would have a chance to replenish, there was no significant deficit in LTP at 4 months. However, under these conditions at 2 months, we see a decrease in paired-pulse ratio following induction of LTP that remains throughout the experiment, indicating an increase in release probability. As outline above, the physiological effect of Aβ is to increase release probability, and so this suggests that the theta rhythm itself may be causing local release of Aβ at the stimulated synapses. Despite this apparent presynaptic increase in transmission, the magnitude of LTP remains unaltered, raising the possibility of a postsynaptic decrease balancing this effect. However, when TEA was applied to slices, resulting in a wide-spread depolarisation and thus release of all neurotransmitter vesicles (excitatory, inhibitory and modulatory), LTP was induced similarly to wild types confirming that some forms of long-term plasticity remain intact. In our hands, the locus of expression of LTP, induced by tetanus, tends to have a presynaptic component in both genotypes, indicated by a change in paired-pulse profile following induction.

Behaviour

In this study, TASTPM mice showed no measurable cognitive deficits at any age, despite a substantial plaque load.

There were, however, clear differences in motor activity and anxiety related behaviours. The TASTPM mice were slower to perform the T-maze task than the wild type mice or failed to do so altogether. Furthermore, in other tests, decreased activity and increased

anxiety were evident. Although not specifically measured, the TASTPM mice are also more aggressive than wild type mice.[41]

The improved retention of learning in TASTPM mice, requiring no repeat training when the same mice were tested twice at 8 and 12 months, may appear counterintuitive. However, similar outcomes in hippocampal learning have been reported in TASTPM mice at around 4 months, using a contextual fear conditioning regime. While mice were unimpaired in learning the task in these previous reports, they failed to extinguish their learnt fear behaviour when conditioning was reversed.[13, 14, 42] In the present study, the difference was additionally noted, with the TASTPM mice also making more correct choices than the wild type mice when a delay between runs was introduced.

The subtlety of the cognitive changes reported here in the TASTPM mouse, even at stages where a heavy plaque load is present, is consistent with previous findings.[13-15, 42] Even when other Aβ models are considered, cognitive deficits are limited and, where present, it is unclear how they truly translate to the human disease (for reviews, see references 43, 44). Moreover, this is consistent with the human condition, where, at the time of diagnosis, when cognitive deficits are first being detected, there is already a substantial reduction in hippocampal volume of up to 20%,[45] whereas there is no apparent neuronal loss in TASTPM mice. Furthermore, in humans, cognitive decline correlates well with Tau PET markers and less with Aβ load.[46] Given that Aβ mouse models are not a complete model of AD, i.e. lacking Tau tangle formation and neurodegeneration, which more faithfully correlate with cognitive decline, they should be considered as models of the preclinical disease, when Aβ is first deposited.

Here we bring together the progression of pathology, microglia, synaptic transmission and other functional changes in a preclinical mouse model of AD. In a following paper we compare these results in mice with only plaques and no neurofibrillary tangles to a transgenic mouse model of later stage dementia in which neurofibrillary tangles occur without plaques.[47]

From the present study we conclude that the earliest effects of Aβ on synaptic transmission are probably due to very low levels of soluble Aβ in the volume of the

tissue, rather than being directly related to plaques. At this early stage plaques are extremely small and sparse so that they would impinge directly on very few synapses. However, while wide-spread soluble Aβ may also influence early microglial changes these may well be influenced by the earliest seeding of plaques. Later changes most probably relate to the increasing numbers of larger plaques with the cloud of high-level soluble Aβ surrounding them impinging on a, still limited, but much greater area. The direct effects of this localised high concentration of soluble Aβ include loss of active synapses and activation of microglia, likely involved in clearing damaged synapses near or within plaques via phagocytosis and thus preventing wider damage to the affected axons and dendrites. While seeding of new plaques seems to continue throughout the development of plaque pathology, it is only once large plaques are present that these latter changes occur. Moreover, the lack of cognitive deficits is similar to the human situation prior to the build-up of neurofibrillary tangles and neurodegeneration and thus suggests that TASTPM represent a good model of the prodromal phase of the disease.

Data sharing

The datasets used and/or analysed during the current study are available from the corresponding author on reasonable request.

Acknowledgements

The authors would like to thank Rivka Steinberg and Stuart Martin for providing genotyping services; Ken Smith, Roshni Desai and Tammaryn Lashley for histological advice; and the Maria Fitzgerald/Steve Hunt laboratories for use of equipment.

Funding

GlaxoSmithKline (FAE); BBSRC Case studentship with GSK to PH (FAE); UCL International Studentship to WL (FAE); ARUK and UCL ARUK Network (FAE, DMC, DAS); MRC (FAE); BBSRC for LM (FC)

A material transfer agreement between GlaxoSmithKline and UCL for use of the TASTPM mice and agreement for the types of experiment was in place prior to experimental design as well as agreement to include GSK authors. GlaxoSmithKline were not involved directly with the design of the experiments. GlaxoSmithKline (JCR) have read and approved the submitted form of the manuscript. No further input was received from funding sources.

Conflicts of Interest

JCR was employed by GlaxoSmithKline during the duration of the experiments performed here in. No further conflicts of interests declared.

Authors' contributions

EM performed the histological staining and counting of microglia and provided feedback on draft manuscript. TB carried out behavioural experiments and analysis and comments on draft manuscript. WL performed the LTP experiments at 12 and 18 months of age and comments on draft manuscript. TH performed LTP and behavioural

experiments at 4 months of age. PH carried out the chemical LTP experiments and comments on draft manuscript. OTJ performed patch clamp experiments for IPSCs at 4 months of age. KY performed the LTP experiments at 24 months. LM provided training and supervision of all behavioural experiments. FM performed LTP experiments at 2 and 4 months of age. MANS performed behavioural experiments at 4 and 8 months of age. GB carried out histological staining and quantification of plaques. RW performed the microglial histology and counting for the TPM mice. JCR developed the mouse model and comments on the draft manuscript. FC designed and supervised the behavioural experiments and provided comments on the draft manuscript. DAS supervised the histological experiments and commented on draft manuscript. DMC supervised all experiments, performed electrophysiological recordings, wrote first draft of the manuscript, performed all statistical analyses, prepared figures, edited and finalised manuscript. FAE obtained funding, designed experiments, edited and finalised manuscript. All authors read and approved the final manuscript.

944 **References**

945 1. Cuyvers E, Sleegers K. Genetic variations underlying Alzheimer's disease:
946 evidence from genome-wide association studies and beyond. *Lancet Neurol* 2016;**15:**
947 857-68. DOI:10.1016/S1474-4422(16)00127-7.
948 2. Hardy J, Allsop D. Amyloid deposition as the central event in the aetiology of
949 Alzheimer's disease. *Trends in Pharmacological Sciences* 1991;**12:** 383-8.
950 3. Blennow K, Mattsson N, Scholl M, Hansson O, Zetterberg H. Amyloid biomarkers
951 in Alzheimer's disease. *Trends Pharmacol Sci* 2015;**36:** 297-309.
952 DOI:10.1016/j.tips.2015.03.002.
953 4. Lewczuk P, Matzen A, Blennow K, et al. Cerebrospinal Fluid Abeta42/40
954 Corresponds Better than Abeta42 to Amyloid PET in Alzheimer's Disease. *J Alzheimers*
955 *Dis* 2017;**55:** 813-22. 10.3233/JAD-160722.
956 5. Abramov E, Dolev I, Fogel H, Ciccotosto GD, Ruff E, Slutsky I. Amyloid-beta as a
957 positive endogenous regulator of release probability at hippocampal synapses. *Nat*
958 *Neurosci* 2009;**12:** 1567-76. DOI:10.1038/nn.2433.
959 6. Dolev I, Fogel H, Milshtein H, et al. Spike bursts increase amyloid-beta 40/42 ratio
960 by inducing a presenilin-1 conformational change. *Nat Neurosci* 2013;**16:** 587-95.
961 DOI:10.1038/nn.3376.
962 7. Iaccarino HF, Singer AC, Martorell AJ, et al. Gamma frequency entrainment
963 attenuates amyloid load and modifies microglia. *Nature* 2016;**540:** 230-5.
964 DOI:10.1038/nature20587.
965 8. Verret L, Mann EO, Hang GB, et al. Inhibitory interneuron deficit links altered
966 network activity and cognitive dysfunction in Alzheimer model. *Cell* 2012;**149:** 708-21.
967 10.1016/j.cell.2012.02.046.
968 9. Selkoe DJ, Hardy J. The amyloid hypothesis of Alzheimer's disease at 25 years.
969 *EMBO Mol Med* 2016;**8:** 595-608. DOI:10.15252/emmm.201606210.
970 10. Matarin M, Salih DA, Yasvoina M, et al. A genome-wide gene-expression analysis
971 and database in transgenic mice during development of amyloid or tau pathology. *Cell*
972 *Rep* 2015;**10:** 633-44. DOI:10.1016/j.celrep.2014.12.041.
973 11. Howlett DR, Bowler K, Soden PE, et al. Abeta deposition and related pathology in
974 an APP x PS1 transgenic mouse model of Alzheimer's disease. *Histol Histopathol*
975 2008;**23:** 67-76. DOI:10.14670/HH-23.67.
976 12. He Z, Guo JL, McBride JD, et al. Amyloid-beta plaques enhance Alzheimer's brain
977 tau-seeded pathologies by facilitating neuritic plaque tau aggregation. *Nat Med* 2018;**24:**
978 29-38. DOI:10.1038/nm.4443.
979 13. Rattray I, Scullion GA, Soulby A, Kendall DA, Pardon MC. The occurrence of a
980 deficit in contextual fear extinction in adult amyloid-over-expressing TASTPM mice is
981 independent of the strength of conditioning but can be prevented by mild novel cage
982 stress. *Behav Brain Res* 2009;**200:** 83-90. DOI:10.1016/j.bbr.2008.12.037.
983 14. Rattray I, Pitiot A, Lowe J, et al. Novel cage stress alters remote contextual fear
984 extinction and regional T2 magnetic resonance relaxation times in TASTPM mice
985 overexpressing amyloid. *J Alzheimers Dis* 2010;**20:** 1049-68. DOI:10.3233/JAD-2010-
986 091354.
987 15. Howlett DR, Richardson JC, Austin A, et al. Cognitive correlates of Abeta
988 deposition in male and female mice bearing amyloid precursor protein and presenilin-1
989 mutant transgenes. *Brain Res* 2004;**1017:** 130-6. DOI:10.1016/j.brainres.2004.05.029.
990 16. Cummings DM, Liu W, Portelius E, et al. First effects of rising amyloid-beta in
991 transgenic mouse brain: synaptic transmission and gene expression. *Brain : a journal of*
992 *neurology* 2015;**138:** 1992-2004. DOI:10.1093/brain/awv127.

17. Richardson JC, Kendal CE, Anderson R, et al. Ultrastructural and behavioural changes precede amyloid deposition in a transgenic model of Alzheimer's disease. *Neuroscience* 2003;**122:** 213-28. 10.1016/S0306-4522(03)00389-0.
18. Cacucci F, Yi M, Wills TJ, Chapman P, O'Keefe J. Place cell firing correlates with memory deficits and amyloid plaque burden in Tg2576 Alzheimer mouse model. *Proc Natl Acad Sci U S A* 2008;**105:** 7863-8. DOI:10.1073/pnas.0802908105.
19. Packard MG, Introini-Collison I, McGaugh JL. Stria terminalis lesions attenuate memory enhancement produced by intracaudate nucleus injections of oxotremorine. *Neurobiol Learn Mem* 1996;**65:** 278-82. 10.1006/nlme.1996.0033.
20. Bliss TVP, Collingridge GL, Morris RG. Synaptic plasticity in health and disease: introduction and overview. *Philos Trans R Soc Lond B Biol Sci* 2014;**369:** 20130129. DOI:10.1098/rstb.2013.0129.
21. Nahum-Levy R, Lipinski D, Shavit S, Benveniste M. Desensitization of NMDA receptor channels is modulated by glutamate agonists. *Biophysical Journal* 2001;**80:** 2152-66.
22. Condello C, Yuan P, Schain A, Grutzendler J. Microglia constitute a barrier that prevents neurotoxic protofibrillar Abeta42 hotspots around plaques. *Nat Commun* 2015;**6:** 6176. DOI:10.1038/ncomms7176.
23. Hong S, Dissing-Olesen L, Stevens B. New insights on the role of microglia in synaptic pruning in health and disease. *Curr Opin Neurobiol* 2016;**36:** 128-34. DOI:10.1016/j.conb.2015.12.004.
24. Guerreiro R, Wojtas A, Bras J, et al. TREM2 variants in Alzheimer's disease. *N Engl J Med* 2013;**368:** 117-27. 10.1056/NEJMoa1211851.
25. Jonsson T, Stefansson H, Steinberg S, et al. Variant of TREM2 associated with the risk of Alzheimer's disease. *N Engl J Med* 2013;**368:** 107-16. 10.1056/NEJMoa1211103.
26. Dagher NN, Najafi AR, Kayala KM, et al. Colony-stimulating factor 1 receptor inhibition prevents microglial plaque association and improves cognition in 3xTg-AD mice. *J Neuroinflammation* 2015;**12:** 139. DOI:10.1186/s12974-015-0366-9.
27. Spangenberg EE, Lee RJ, Najafi AR, et al. Eliminating microglia in Alzheimer's mice prevents neuronal loss without modulating amyloid-beta pathology. *Brain : a journal of neurology* 2016;**139:** 1265-81. DOI:10.1093/brain/aww016.
28. Olmos-Alonso A, Schetters ST, Sri S, et al. Pharmacological targeting of CSF1R inhibits microglial proliferation and prevents the progression of Alzheimer's-like pathology. *Brain : a journal of neurology* 2016;**139:** 891-907. 10.1093/brain/awv379.
29. Sosna J, Philipp S, Albay R, 3rd, et al. Early long-term administration of the CSF1R inhibitor PLX3397 ablates microglia and reduces accumulation of intraneuronal amyloid, neuritic plaque deposition and pre-fibrillar oligomers in 5XFAD mouse model of Alzheimer's disease. *Mol Neurodegener* 2018;**13:** 11. DOI:10.1186/s13024-018-0244-x.
30. Hong S, Beja-Glasser VF, Nfonoyim BM, et al. Complement and microglia mediate early synapse loss in Alzheimer mouse models. *Science* 2016;**352:** 712-6. DOI:10.1126/science.aad8373.
31. Spires TL, Meyer-Luehmann M, Stern EA, et al. Dendritic spine abnormalities in amyloid precursor protein transgenic mice demonstrated by gene transfer and intravital multiphoton microscopy. *J Neurosci* 2005;**25:** 7278-87. DOI:10.1523/JNEUROSCI.1879-05.2005.
32. Kirkwood CM, Ciuchta J, Ikonomovic MD, et al. Dendritic spine density, morphology, and fibrillar actin content surrounding amyloid-beta plaques in a mouse model of amyloid-beta deposition. *J Neuropathol Exp Neurol* 2013;**72:** 791-800. DOI:10.1097/NEN.0b013e31829ecc89.

1043 33. Edwards FA. Anatomy and electrophysiology of fast central synapses lead to a
1044 structural model for long-term potentiation. *Physiological Reviews* 1995;**75:** 759-87.
1045 34. Zhang Y, Li P, Feng J, Wu M. Dysfunction of NMDA receptors in Alzheimer's
1046 disease. *Neurol Sci* 2016;**37:** 1039-47. DOI:10.1007/s10072-016-2546-5.
1047 35. Kamenetz F, Tomita T, Hsieh H, et al. APP processing and synaptic function.
1048 *Neuron* 2003;**37:** 925-37.
1049 36. Cirrito JR, Kang JE, Lee J, et al. Endocytosis is required for synaptic activity-
1050 dependent release of amyloid-beta in vivo. *Neuron* 2008;**58:** 42-51.
1051 DOI:10.1016/j.neuron.2008.02.003.
1052 37. Cirrito JR, Yamada KA, Finn MB, et al. Synaptic activity regulates interstitial fluid
1053 amyloid-beta levels in vivo. *Neuron* 2005;**48:** 913-22.
1054 DOI:10.1016/j.neuron.2005.10.028.
1055 38. Parent A, Linden DJ, Sisodia SS, Borchelt DR. Synaptic transmission and
1056 hippocampal long-term potentiation in transgenic mice expressing FAD-linked
1057 presenilin 1. *Neurobiol Dis* 1999;**6:** 56-62. 10.1006/nbdi.1998.0207.
1058 39. Dewachter I, Ris L, Croes S, et al. Modulation of synaptic plasticity and Tau
1059 phosphorylation by wild-type and mutant presenilin1. *Neurobiology of Aging* 2008;**29:**
1060 639-52.
1061 40. Auffret A, Gautheron V, Repici M, et al. Age-dependent impairment of spine
1062 morphology and synaptic plasticity in hippocampal CA1 neurons of a presenilin 1
1063 transgenic mouse model of Alzheimer's disease. *JNS* 2009;**29:** 10144-52.
1064 41. Pugh PL, Richardson JC, Bate ST, Upton N, Sunter D. Non-cognitive behaviours in
1065 an APP/PS1 transgenic model of Alzheimer's disease. *Behav Brain Res* 2007;**178:** 18-28.
1066 DOI:10.1016/j.bbr.2006.11.044.
1067 42. Pardon MC, Sarmad S, Rattray I, et al. Repeated novel cage exposure-induced
1068 improvement of early Alzheimer's-like cognitive and amyloid changes in TASTPM mice
1069 is unrelated to changes in brain endocannabinoids levels. *Neurobiol Aging* 2009;**30:**
1070 1099-113. DOI:10.1016/j.neurobiolaging.2007.10.002.
1071 43. Foley AM, Ammar ZM, Lee RH, Mitchell CS. Systematic review of the relationship
1072 between amyloid-beta levels and measures of transgenic mouse cognitive deficit in
1073 Alzheimer's disease. *J Alzheimers Dis* 2015;**44:** 787-95. DOI:10.3233/JAD-142208.
1074 44. Kobayashi DT, Chen KS. Behavioral phenotypes of amyloid-based genetically
1075 modified mouse models of Alzheimer's disease. *Genes Brain Behav* 2005;**4:** 173-96.
1076 DOI:10.1111/j.1601-183X.2005.00124.x.
1077 45. Ridha BH, Barnes J, Bartlett JW, et al. Tracking atrophy progression in familial
1078 Alzheimer's disease: a serial MRI study. *Lancet Neurol* 2006;**5:** 828-34.
1079 DOI:10.1016/S1474-4422(06)70550-6.
1080 46. Brier MR, Gordon B, Friedrichsen K, et al. Tau and Abeta imaging, CSF measures,
1081 and cognition in Alzheimer's disease. *Sci Transl Med* 2016;**8:** 338ra66.
1082 DOI:10.1126/scitranslmed.aaf2362.
1083 47. Joel Z, Izquierdo P, Liu W, et al. A TauP301L mouse model of dementia;
1084 development of pathology, synaptic transmission, microglial response and cognition
1085 throughout life. *bioRxiv* 2018;**420398:** DOI:10.1101/420398.
1086

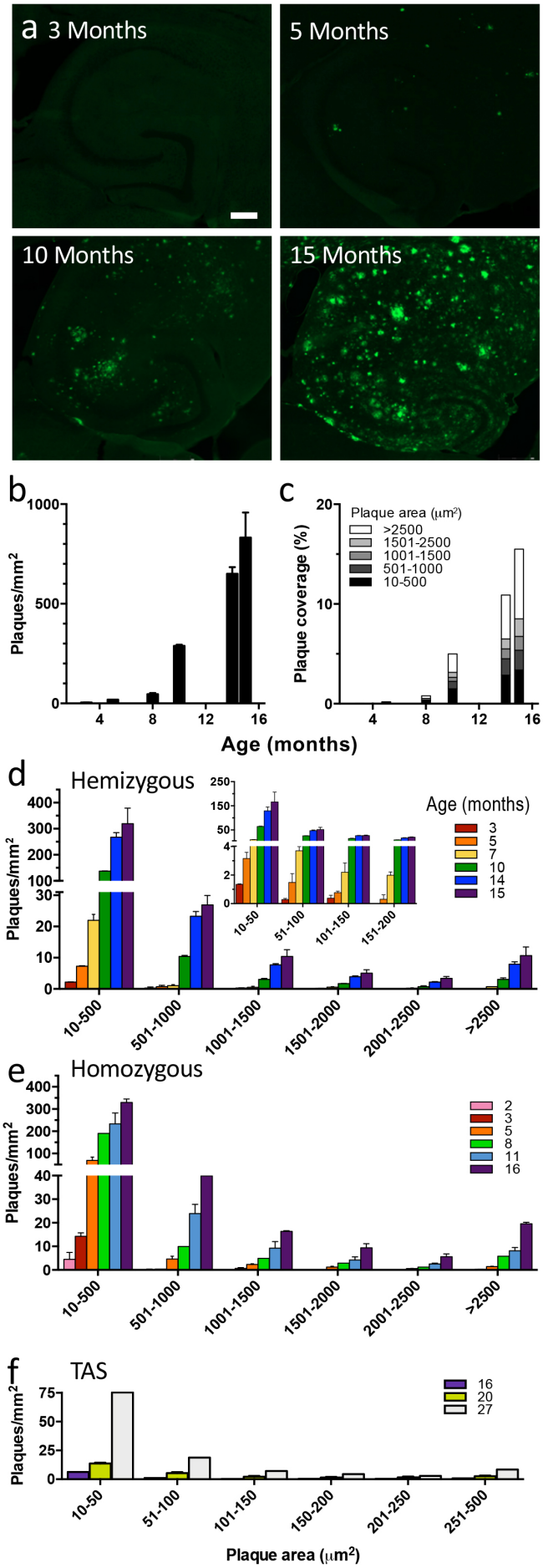
a 3 Months
5 Months
10 Months
15 Months
b
Plaques/mm²
Age (months)
c
Plaque coverage (%)
Plaque area (μm²)
>2500
1501-2500
1001-1500
501-1000
10-500
d
Hemizygous
Age (months)
3
5
7
10
14
15
10-50
51-100
101-150
151-200
10-500
501-1000
1001-1500
1501-2000
2001-2500
>2500
e
Homozygous
2
3
5
8
11
16
f
TAS
16
20
27
10-50
51-100
101-150
150-200
201-250
251-500
Plaque area (μm²)

1087

1088 **Figure 1 Plaque development in TASTPM mice**

1089 a) Representative micrographs of Aβ40 (green) immunofluorescence in hippocampus
1090 from 3- to 15-month-old hemizygous TASTPM mice. Scale bar 250 μm. b) Plaque density
1091 measured at different ages in TASTPM mice (n=2-3 animals per age group). c)
1092 Proportion of plaques of indicated sizes contributing to increased percentage coverage
1093 of the hippocampus with increased age. d) Density of plaques within specific size ranges
1094 (as indicated on x-axes) over age (colours as indicated in key). The inset covers smaller
1095 bin sizes for plaques up to 200 μm^2. Note the split y-axes. e) Density of homozygous
1096 TASTPM plaques within specific size ranges (as indicated on x-axes) over age (colours as
1097 indicated in key). f) Density of TAS plaques within specific size ranges (as indicated on x-
1098 axes) over age (colours as indicated in key). Note the different x and y-axes in f
1099 compared to d and e, with few plaques and maximum plaque area under 500 μm^2. All
1100 data are represented by mean±SEM.

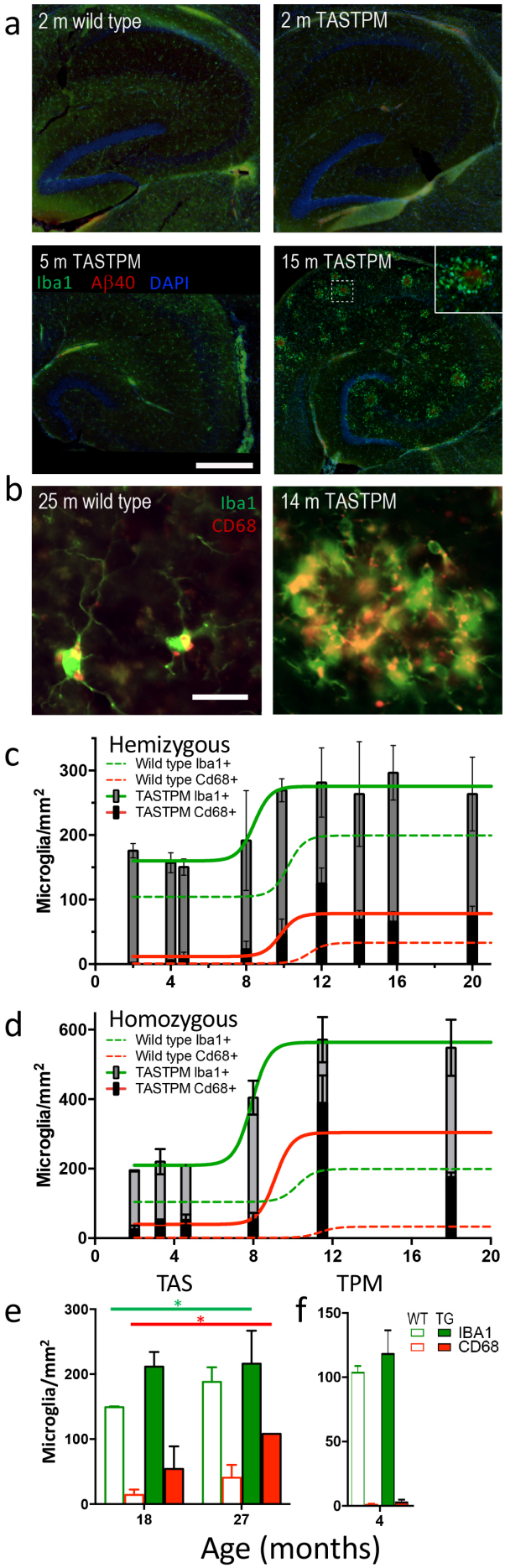
a
2 m wild type
2 m TASTPM
5 m TASTPM
Iba1 Aβ40 DAPI
15 m TASTPM
b
25 m wild type
Iba1
CD68
14 m TASTPM
c
Hemizygous
Wild type Iba1+
Wild type Cd68+
TASTPM Iba1+
TASTPM Cd68+
Microglia/mm²
d
Homozygous
Wild type Iba1+
Wild type Cd68+
TASTPM Iba1+
TASTPM Cd68+
Microglia/mm²
TAS
TPM
e
Microglia/mm²
f
WT TG
IBA1
CD68
Age (months)

1101

1102 **Figure 2 Microglial proliferation and activation in TASTPM mice**

1103 a) Microglia (Iba1, green) cluster around plaques (Aβ1-40, red) in TASTPM mouse
1104 hippocampus (nuclei: DAPI, blue). Scale bar 250 μm. b) Examples of phagocytic
1105 microglia (CD68, red + Iba1, green; yellow when colocalised) in wild type and TASTPM
1106 hippocampus. Scale bar 25 μm. c) Total microglial density (Iba1+, full bar height) and
1107 phagocytic microglial (Iba1 + CD68+, black bar) density in hemizygous TASTPM mice
1108 with age. Sigmoidal fits are shown (Iba1 green; CD68 red): unbroken lines, TASTPM;
1109 dashed lines, wild type (only fit shown for wild type). d) Total and phagocytic microglial
1110 densities in homozygous TASTPM mice with age. Sigmoidal fits are shown. e) Total and
1111 phagocytic microglial densities in the APP_{Swe} TAS mice at the ages shown. Significant
1112 main effects of genotype for both IBA1 and CD68 are indicated by *$p<0.05$. f) Densities of
1113 total microglia and CD68 positive phagocytic microglia in 4 month old $PSEN1_{M146V}$ TPM
1114 microglia. All data are represented by mean±SEM.

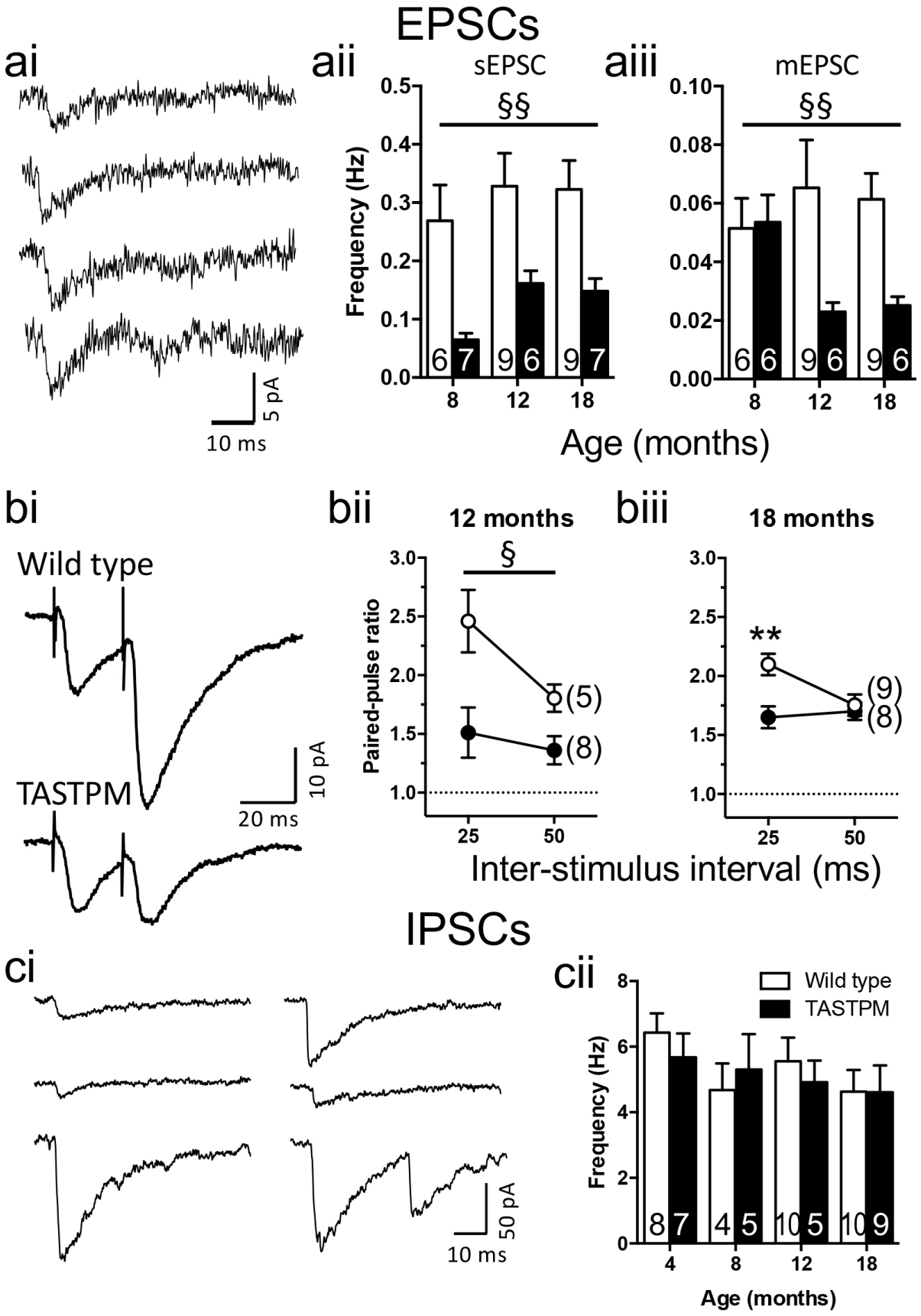
EPSCs
ai
aii
sEPSC
aiii
mEPSC
§§
§§
Frequency (Hz)
5 pA
10 ms
Age (months)
bi
bii
12 months
biii
18 months
Wild type
TASTPM
10 pA
20 ms
§
**
Paired-pulse ratio
Inter-stimulus interval (ms)
IPSCs
ci
cii
Wild type
TASTPM
50 pA
10 ms
Frequency (Hz)
Age (months)

1115

Figure 3 Excitatory and inhibitory synaptic transmission in TASTPM mice

ai) Example spontaneous and miniature EPSCs recorded from 18-month-old TASTPM. aii) Frequency of spontaneous EPSCs. Main effect of genotype by 2-way ANOVA ($p=0.0011$). aiii) Frequency of miniature EPSCs. Main effect of genotype by 2-way ANOVA ($p < 0.01$) bi) Example responses evoked by paired stimuli. bii) Paired-pulse ratios from 12-month-old mice. Main-effect of genotype by 2-way ANOVA ($p=0.02$). (biii) Paired-pulse ratios from 18-month-old mice. Genotype by inter-stimulus interval interaction ($p<0.05$); Sidak post-hoc test is indicated ($p=0.002$). ci) Example continuous recordings of spontaneous IPSCs. cii) Spontaneous IPSC frequencies. Sample sizes are indicated by the numbers within bars or within parentheses. * $p<0.05$; ** $p<0.01$. All data are represented by mean±SEM.

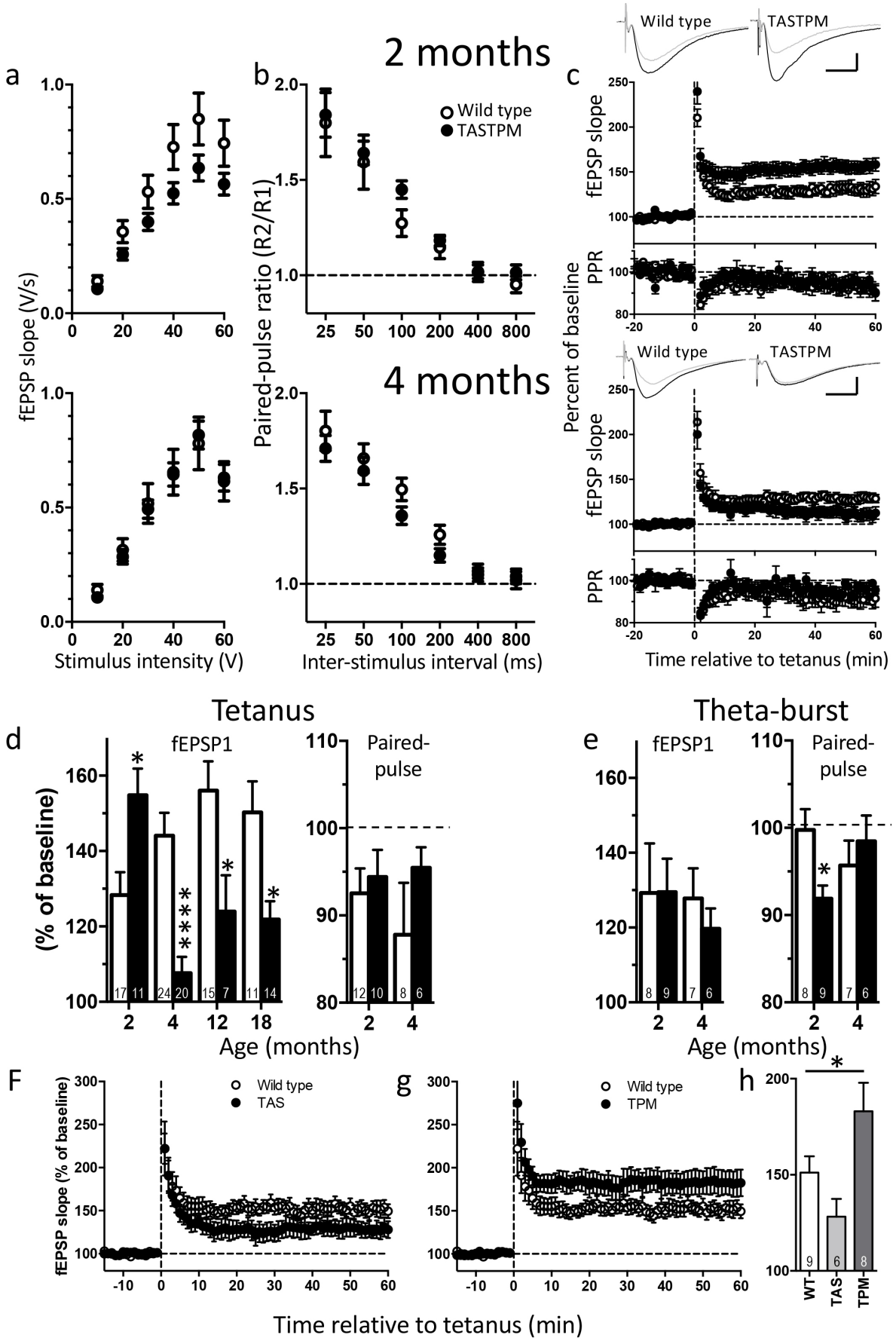
2 months
4 months
a
b
c
fEPSP slope (V/s)
Stimulus intensity (V)
Paired-pulse ratio (R2/R1)
Inter-stimulus interval (ms)
Wild type
TASTPM
Percent of baseline
fEPSP slope
PPR
Time relative to tetanus (min)
Tetanus
Theta-burst
d
e
fEPSP1
Paired-pulse
(% of baseline)
Age (months)
F
g
h
Wild type
TAS
TPM
fEPSP slope (% of baseline)
Time relative to tetanus (min)
WT
TAS
TPM

1127

1128 **Figure 4 Field EPSP recordings of synaptic plasticity in TASTPM mice**
1129 a-c) 2 months upper row; 4 months lower row. a) Input-output relationship, b) Paired-
1130 pulse ratio profile and c) Time course of tetanus-induced LTP: fEPSP (upper panels) and
1131 paired-pulse ratio (PPR, lower panels) after induction as a percentage of pre-induction
1132 baseline. Traces are representative fEPSPs from baseline (grey) and the 51-60 minutes
1133 after tetanus (black). Scale bars: 5 ms x 0.5 mV. d) Magnitude of LTP (*left*) induced by
1134 tetanus over 2-18 months of age (number of mice as indicated in each column). Two-
1135 way ANOVA revealed significant age x genotype interaction ($P<0.0001$). Change in
1136 paired-pulse ratio (*right*) following LTP induction. Both wild type and TASTPM mice
1137 showed a significant decrease in PPR compared to baseline at both ages (paired t-tests
1138 within separate experiments; $p < 0.05$). No significant difference between genotypes
1139 (two-way ANOVA). e) Magnitude of LTP induced by theta-burst stimulation (*left,* no
1140 significant difference between genotypes) and corresponding change in paired-pulse
1141 ratio (*right*; two-way ANOVA age x genotype interaction $p < 0.05$). Sidak post hoc test:
1142 *$P<0.05$; ****$P<0.0001$. f) LTP induced by tetanic stimulation in APP_{Swe} TAS mice at 24
1143 months of age. g) LTP induced by tetanic stimulation in $PSEN1_{M146V}$ TPM mice at 24
1144 months. Wild type animals are common to both panels f and g. h) Magnitude of LTP
1145 induced in 24 month old wild type, TAS and TPM mice. 24 month old recordings for all
1146 genotypes were interleaved; significance tested by one-way ANOVA, *$p<0.05$. All data
1147 are represented by mean±SEM.

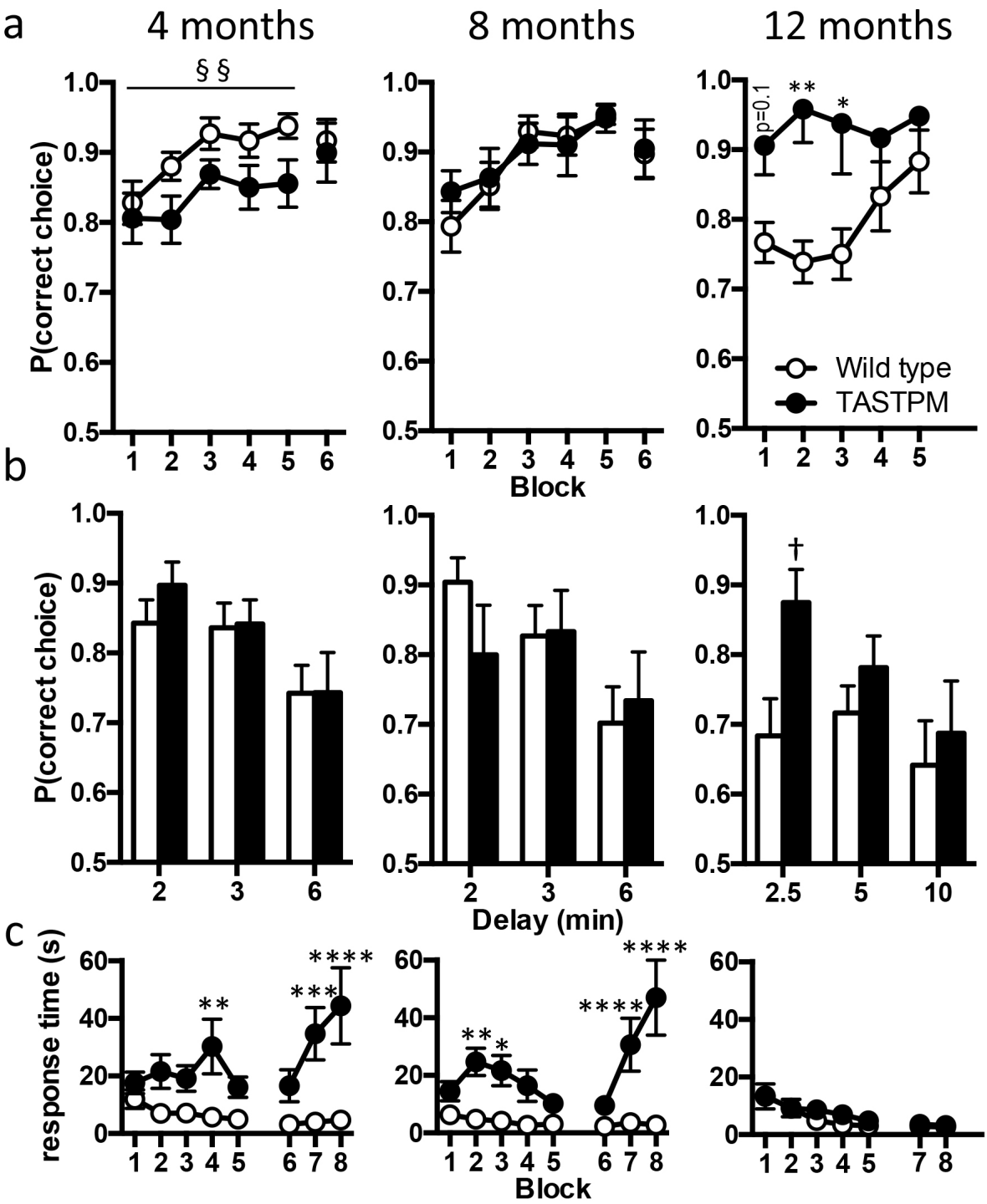
a
4 months
8 months
12 months
§ §
p=0.1
**
*
P(correct choice)
Wild type
TASTPM
Block
b
†
Delay (min)
c
response time (s)
****
***
**
*
Block

1148

Figure 5 Hippocampus-dependent T-Maze learning in TASTPM mice

a-c) Ages as indicated above panel a. a) Probability of mice making a correct choice in the choice run at 4 months (n=15-16 animals completing the task), 8 months (n=10-13 animals completing the task) and 12 months of age (wild type n=15; TASTPM n=8). At 4 months of age there was a main effect of genotype in a two-way ANOVA (§§ $p<0.01$). Note the difference in starting performance at 12 months of age. These are the same mice tested at 8 months. As expected wild type mice started at around 75% correct choices and improved with training having, extinguished their previous training. TASTPM mice unexpectedly started training making correct choices 90% of the time having retained the previous improved level. Two-way ANOVA interaction between training block and genotype ($p<0.03$); Sidak post hoc analyses are indicated by *$P<0.05$, **$P<0.01$. b) The introduction of delays between sample and choice runs revealed no further differences between genotypes at 4 or 8 months of age, while at 12 months, a significant effect of genotype was observed with TASTPM mice retaining performance despite a 2.5 minute delay before the choice run († $p<0.05$). c) Response time for choice run at 4 -12 months of age, Sidak post hoc analyses are indicated by *$P<0.05$, **$P<0.01$, ***$P<0.001$, ****$P<0.0001$. All data are represented by mean±SEM.

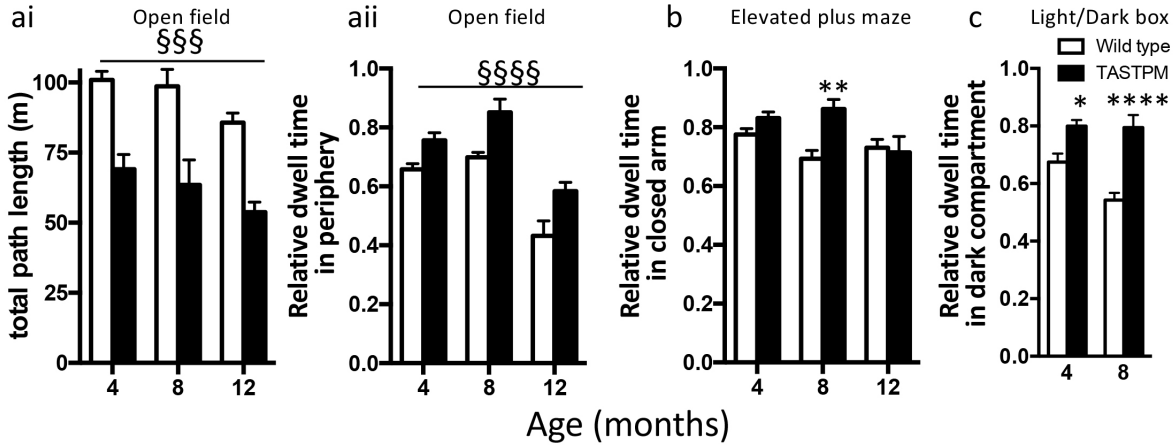

Figure 6 Open field and tests of anxiety

a) Open field test. ai) Total path length run over 30 mins. Main effect of genotype by two-way ANOVA (§§§ p<0.001). aii) Time spent in peripheral area. Main effect of genotype by two-way ANOVA (§§§§ p<0.0001). b) Elevated plus maze. Relative time in closed arm. c) Light/dark box. Relative time spent in dark compartment (12 months not tested.) In b and c, Sidak post hoc tests are indicated (two-way ANOVA genotype x age interaction P<0.05; * p<0.05; ***p<0.001; **** p<0.0001). All data are represented by mean±SEM.

1175 **Table 1:** *Antibodies used for immunohistochemistry:*

Antibody	Dilution	Source	RRID
IBA1	1:500	Wako (019-19741)	AB_839504
CD68	1:500	BioRad (MCA1957)	AB_322219
Aβ1-40	1:300	ThermoFisher (44-136)	AB_2533599

1176